Title	Local interfacial structure influences charge localization in titania composites: Beyond the band alignment paradigm
Authors	Nolan, Michael;Deskins, N. Aaron;Schwartzenberg, Kevin C.;Gray, Kimberly A.
Publication date	2016-01
Original Citation	Nolan, M., Deskins, N. A., Schwartzenberg, K. C. and Gray, K. A. (2016) 'Local Interfacial Structure Influences Charge Localization in Titania Composites: Beyond the Band Alignment Paradigm', The Journal of Physical Chemistry C, 120(3), pp. 1808-1815. 10.1021/acs.jpcc.5b12326
Type of publication	Article (peer-reviewed)
Link to publisher's version	10.1021/acs.jpcc.5b12326
Rights	© 2016 American Chemical Society. ACS AuthorChoice - This is an open access article published under an ACS AuthorChoice License, which permits copying and redistribution of the article or any adaptations for non-commercial purposes. - http://pubs.acs.org/page/policy/authorchoice_termsofuse.html
Download date	2025-09-03 04:59:21
Item downloaded from	https://hdl.handle.net/10468/4941

Local Interfacial Structure Influences Charge Localization in Titania Composites: Beyond the Band Alignment Paradigm

Michael Nolan*

Tyndall National Institute, University College Cork, Lee Maltings, Cork, Ireland

N. Aaron. Deskins

Department of Chemical Engineering, Worcester Polytechnic Institute, 100 Institute Road, Worcester, Massachusetts 01609, United States

Kevin C. Schwartzenberg and Kimberly A. Gray

Department of Civil and Environmental Engineering, Northwestern University, Evanston, Illinois 60208, United States

ABSTRACT: The phase junction of nanocomposite materials is key to enhanced performance but is largely ignored in recent theoretical examinations of photocatalytic interactions in titania-based composites. Computational advances now allow more precise modeling of the electronic and optical properties of composites, and focusing on mixed-phase TiO_2 as a model, we use density functional theory (DFT) to interrogate the essential structural feature, namely, the rutile−anatase interface, and its relationship to photogenerated charge localization, bulk band alignments, and defect formation. The interfacial region is disordered and distinct from rutile and anatase and contains low coordinated Ti sites and oxygen vacancies, both drivers of charge localization. The relaxations of the interface upon formation of excited electrons and holes determine the final location of charges which cannot always be predicted from bulk band alignments. A detailed understanding of the interfacial phase junction lays the foundation for directed synthesis of highly active and efficient composite photocatalysts.
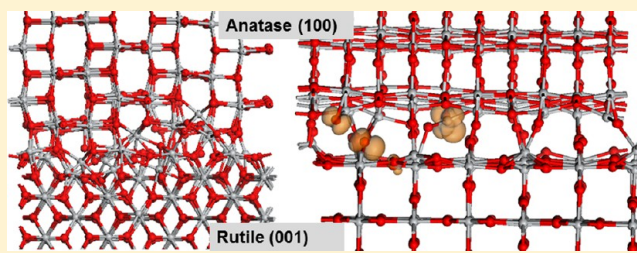
1. INTRODUCTION

Heterojunctions often impart superior reactivity over the individual components in composite materials.[1−13] This is particularly true for mixed-phase TiO_2, where it is well established that interwoven anatase and rutile crystallites display much higher photoactivity than either pure phase alone.[14−16] Proposed explanations for this behavior include charge transfer, separation, or trapping to hinder recombination and prolong carrier lifetimes, extended photoresponse to harvest visible light, and creation of interfacial, under-coordinated or defect sites that serve as catalytic "hot spots".[16] Yet, a theoretical examination of heterojunction structure and its effect on charge localization has not been successfully addressed and is required in order to tailor photoactive material design.

Previous controversy about the relative position of band edges and the direction of charge transfer in anatase/rutile composites[14,17−22] has been resolved experimentally[16,23−27] and by recent theoretical studies.[28−32] The relative positions of bulk band edges between anatase and rutile are aligned using density functional theory (DFT) to show consistently that the rutile conduction band minimum and valence band maximum lie above those of anatase.[28,31] Scanlon et al. reported similar

results using hybrid DFT and a quantum-mechanical/molecular-mechanical (QM/MM) embedding approach in combination with high-resolution XPS.[32] Thus, photogenerated electrons should migrate from rutile to anatase and holes from anatase to rutile.

These studies, however, focus only on bulk energy band alignments, neglecting other factors including the structure of the anatase−rutile interface, which, given the unique atomic and electronic properties at the heterojunction, can influence band offsets.[33] Furthermore, the geometry of the interfacial region may induce the formation of trapping sites and dipoles, which also affect the band structure.[34] Models of the anatase−rutile interface are disordered with Ti having a range of coordination numbers. Kullgren et al. found it dominated by tetrahedrally coordinated Ti species.[30] Garcia et al. reported similar results for band offsets using single-point DFT+U simulations in a model of anatase−rutile interfaces using large surface slabs and supercells containing thousands of atoms generated from simulated annealing, which allow relaxations and rearrangements to reduce excess strain and produce 4-

coordinate Ti species in the interfacial region; e.g. Figure 7 in ref 29 highlights some 4-coordinate Ti species.

While simulations highlight the importance of interfacial distortions in local atomic structure, the experimental literature has long stressed the importance of defects at the anatase–rutile phase junction.[34−37] Excess charge relocation depends strongly on surface structure[34] and distorted surface structures such as 4-fold coordinated Ti to accommodate excess charges introduced by photoexcited charge carriers or defects (e.g., O-vacancy induced band gap states).[36−38] Interfacial defects in anatase bilayers are more stable than surface defects and display a larger effect on inhibiting charge recombination, increasing the surface concentration of photogenerated charge carriers.[36,38]

First-principles simulations help resolve the complexities revealed by experimental interrogation of the interface.[29,30] We hypothesize that the interfacial structure in mixed-phase TiO_2 determines electronic behavior and hence enhanced photocatalytic performance. We conduct a DFT analysis of models of mixed-phase TiO_2 and discuss the geometry of nonbulk-like interfacial regions to illustrate that photoexcited charges localize at certain defects. Our results show for the first time that holes localize at interfacial oxygen, and the presence of under-coordinated Ti provides favorable sites for electron trapping, similar to ref 29. Furthermore, given the localization pattern of the photoexcited electron and valence band hole in the rutile(001)–anatase(100) interface, ignoring local interfacial features can lead to erroneous conclusions regarding the direction of electron and hole flow, and thus the details of the interfacial region are crucial to explaining the fundamental origin of the enhanced photocatalytic activity in anatase–rutile composites.

2. METHODS

Density functional theory calculations on the rutile–anatase interface models were performed with the VASP.5.2 code[39,40] using three-dimensional periodic boundary conditions in a plane wave basis set describing the valence electrons and a cutoff energy of 400 eV. Projector augmented wave potentials[41] were used to describe the core−valence interactions, with 4 and 6 valence electrons on Ti and O, respectively. The PBE exchange-correlation functional[42] was used, with that addition of a correction for on-site Coulomb interactions (PBE+U) that is by now accepted as necessary to describe localized Ti^{3+} states. We use U = 4.5 eV throughout the paper to capture electron localization on Ti sites. There is of course no single value of U that will describe all properties of a material such as TiO_2 perfectly, and the choice of this particular value of U is motivated by describing consistently electron localization after both photoexcitation and oxygen vacancy formation. However, the properties of TiO_2 can and do depend on the choice of U value, and the literature describes a range of values for different studies, which we have summarized in our previous work in ref 29. There it was shown that a wide range of U values, including different +U corrections on rutile and anatase, will not modify the key ground state properties of the rutile−anatase interfaces. Thus, we focus on values of U that give valid charge localization. Large values of U can give charge localization but will move the defect states into the valence band region, which is obviously incorrect. There is thus a narrow range of values of U that can be considered in modeling charge localization in these interface models.

A final point in considering the DFT+U approach is that although ref 42 shows that upon oxygen vacancy formation electron localization is favored in bulk rutile, bulk anatase appears to favor electron delocalization, and a value of U = 3.9 eV was therefore recommended for bulk anatase (while maintaining charge localization in rutile). However, in the interface models used in this work the interfacial atomic structure deviates strongly from that of perfect bulk rutile and anatase, and the corresponding surfaces and the charge localization/delocalization will not necessarily follow the trends from the corresponding bulk materials. To investigate if the choice of U has any effect on the charge localization, we have performed another calculation of the photoexcited state in the rutile(001)−anatase(100) interface using U = 3.9 eV from ref 42, and this is described in Section 3.2. We note that the size of the interface models that we use makes a screening of many different DFT+U setups extremely computationally demanding, without necessarily adding any new insights into these studies. The most important point is that the DFT+U setup is able to describe charge localization in the interface so as to be consistent with experimental findings.

In all calculations, unless stated, the atomic positions were relaxed, with convergence in the forces of 0.02 eV/Å. Given the size of the surface supercells in the calculation, gamma point sampling was used. The interface models are constructed as described elsewhere[29,44] using near coincidence lattice site theory (NCSL) but were relaxed within the DFT+U setup described above. The rutile(110)−anatase(101) and rutile(001)−anatase(100) interface models have dimensions in the interface plane of 20.5 × 19.29 Å and 18.2 × 22.7 Å, significantly larger than usually used in modeling TiO_2 surfaces. The interfaces will be denoted R(110)−A(101) and R(001)−A(100) in what follows.

2.1. Photoexcited State Model. To examine the important questions of (1) where the photoexcited electron and hole will be localized (in the interface or in the individual bulk regions) and (2) what are the localization and energies associated with electron and hole trapping, we use a model in which a triplet electronic state is imposed.[45−48] In this model, the triplet electronic state (with the same number of electrons as the ground state, but now with two electrons having the same spin) places an "excited" electron in the CB and a hole in the VB, and we can investigate the geometric and electronic structure associated with this electronic state. The setup used in this model has been described previously,[45−48] and here we note that in addition to using DFT+U for Ti 3d states we apply a +U correction, where U = 5.5 eV, on the O 2p states to give VB-hole localization.[47,48] To calculate the trapping energy and the singlet−triplet excitation energy, three energies are required:

- the energy of the relaxed singlet ground state, giving $E^{singlet}$
- a single-point energy of the triplet electronic state at the singlet ground state geometry, giving $E^{unrelaxed}$
- a full ionic relaxation of the triplet electronic state, $E^{relaxed}$.

A dipole correction perpendicular to the surface plane is added to the total energies. The vertical excitation energy (corresponding to the VB−CB energy gap from the DOS) is $E^{vertical} = E^{unrelaxed} − E^{singlet}$, while the singlet−triplet excitation energy is $E^{S-T} = E^{singlet} − E^{relaxed}$. The change in this energy with respect to the bare surface allows us to determine the effect of the surface modification on the energy gap of TiO_2, as an
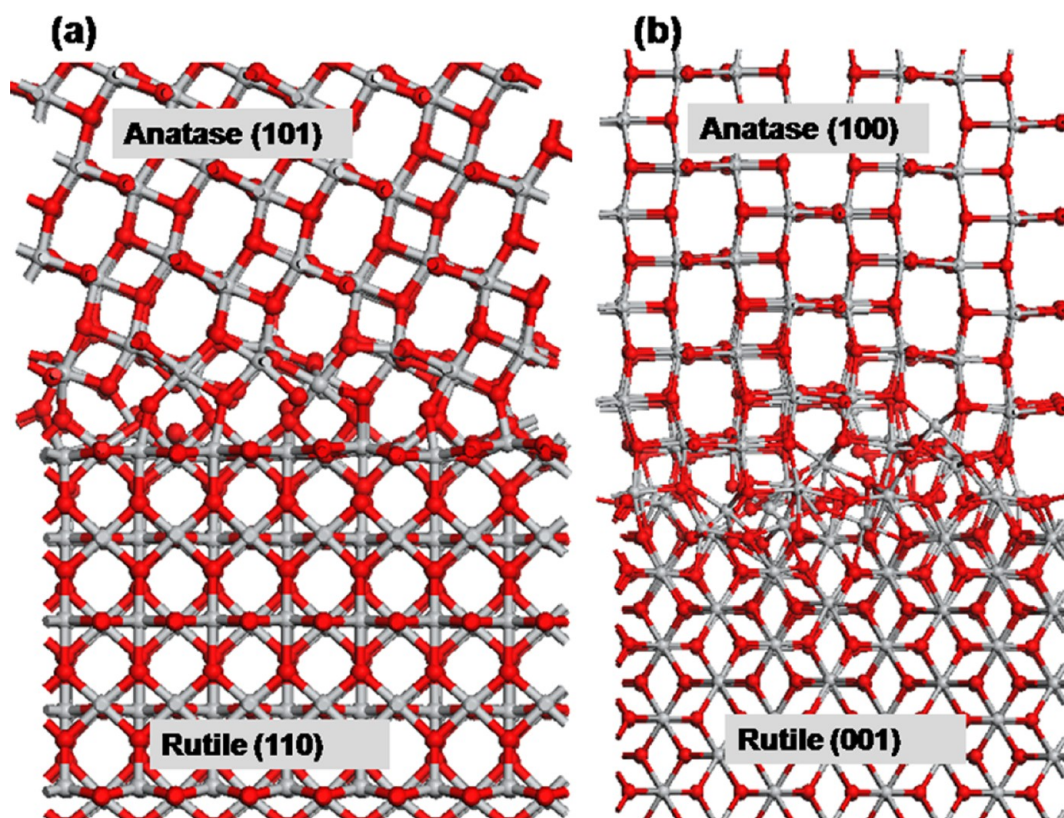
Figure 1. Atomic structures of (a) R(110)−A(101) and (b) R(001)−A(100) interface models. Structures fully relaxed with the DFT+U setup described in the text. In this and in all subsequent figures, Ti is indicated by gray spheres and O by red spheres.

approximation to the excitation energy. The triplet relaxation (carrier trapping) energy is $E^{relax} = E^{relaxed} - E^{unrelaxed}$ and is the energy gained when the electron and hole are trapped at their Ti and O sites upon structural relaxation. We note that in the relaxed triplet electronic state the interface atomic structure can change in response to any charge localization that occurs.

2.2. Oxygen Vacancy Formation. We model oxygen vacancy formation by removing a neutral oxygen vacancy from the interface region and examine two representative oxygen sites. One oxygen is from the original rutile slab, and the other is from the original anatase slab. We compute the oxygen vacancy formation energy from

$$E^{vac} = \left[E^{Defective} + \frac{1}{2}E^{O_2} \right] - E^{Nondefective}$$

where E^{vac} is the vacancy formation energy; $E^{defective}$ is the energy of mixed-phase TiO$_2$ with the vacancy; and $E^{nondefective}$ is the energy of the pristine mixed-phase TiO$_2$.

3. RESULTS

3.1. Models of TiO$_2$ Rutile−Anatase Interfaces. We study two models of mixed-phase TiO$_2$ that allow for reasonable lattice matching, namely, rutile(110)−anatase(101) and rutile(001)−anatase(100),[29,43] hereafter are referred to as R(110)−A(101) and R(001)−A(100). The atomic structures of the R(110)−A(101) and R(001)−A(100) interfaces are fully relaxed within the DFT+U approximation, having previously been relaxed using a molecular dynamics (MD) procedure;[29,43] these structures formed the starting structures for the DFT+U ground state relaxation. In our earlier work[29] the DFT+U calculations were performed at the geometry obtained from the

MD simulations. The relaxed atomic structures of the interface models are shown in Figure 1. The supercells used for the R(110)−A(101) and R(001)−A(100) interface models have dimensions in the interface plane of 20.5 × 19.29 and 18.2 × 22.7 Å, which are sufficiently large to minimize lattice mismatch, and hence strain, between the interfaced surfaces and to give interface atoms freedom to relax to obtain more favorable local coordination environments.

In the interfacial structures shown in Figure 1, rutile and anatase phases are evident, with a disordered region present at the rutile−anatase junction. To examine this in more detail, Figure 2 shows the interfacial region in which under-coordinated Ti sites are highlighted, while the remaining Ti atoms are 5- and 6-fold coordinated. There is no unambiguous way to assign a coordination to a given species, and so we use a reasonable approach that if a Ti−O distance in the ground states (with only Ti^{4+} present) is larger than 2.10 Å then the Ti and O are not coordinated. This is reasonable given that bulk TiO$_2$ and surfaces do not show any Ti−O distances larger than 2.10 Å. The structural characteristics of disordered R−A interfaces from MD simulations have been described.[29,43] For this paper, we are interested in the details of undercoordinated Ti and O species in the interfacial region.

The Ti−O distances around undercoordinated Ti sites range from 1.98 to 2.09 Å in R(110)−A(101) and 1.90 to 2.09 Å in R(001)−A(100), which are typical of Ti−O distances involving 4-coordinated Ti species.[50,51] From earlier work on interfaces and TiO$_2$ nanostructures, such Ti sites are believed to be favorable sites for electron localization[29,30,34,49−51] We find that of the 2-fold coordinated oxygen from the original rutile and anatase phases most interfacial oxygens remain 2-fold
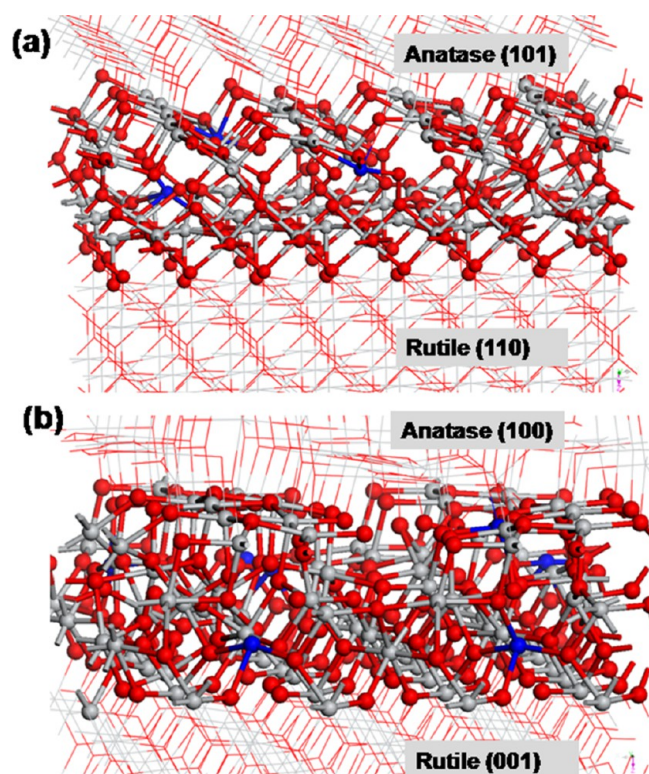
Figure 2. Local atomic structure in the R−A interface models, highlighting Ti sites with 4-fold coordination. These Ti atoms are indicated by the blue spheres. (a) R(110)−A(101) interface and (b) R(001)−A(100) interface.

coordinated with some taking 3-fold coordination. There are no singly coordinated titanyl species present in the interface.

The energy band alignments can be studied from the electronic density of states. Since our findings with these interface models are consistent with the general consensus[28,30−32] and have been discussed previously,[29] we only briefly mention the key results to prepare for the discussion in Section 2.2. In the present rutile−anatase interface models, the VB_{max} for atoms from the interface lies higher in energy than the VB_{max} for the bulk atoms, by 0.4−0.6 eV, depending on the rutile and anatase crystal plane present in the interface model. The conduction CB_{min} for the interfacial region lies at slightly higher energy than the bulk CB_{min} with the rutile derived CB_{min} lying 0.15 eV higher in energy than the anatase derived CB_{min}. While there are some quantitative differences compared to previous work,[28−32] the qualitative findings regarding band alignments are consistent.

From these band alignments, we expect electrons to localize on Ti atoms originating from anatase and holes to localize on oxygen sites originating from rutile. However, this analysis fails to explain relaxations in the interface structure upon formation and localization of an excited electron−hole pair or the creation of point defects, such as oxygen vacancies. Interrogation of these key aspects of TiO_2 interfaces will allow us to directly compare our models to experimental results to understand the microscopic process at work in mixed-phase TiO_2.

3.2. Electron and Hole Localization in a Model of Photoexcited Mixed-Phase TiO_2. To model the formation of an excited electron and hole pair in mixed-phase TiO_2, we construct a simple system with a triplet electronic state that mimics the formation of an electron in the conduction band

and a hole in the valence band of TiO_2. This model has been used successfully in studies of rutile and anatase surfaces,[44−47] in hole scavenging on anatase (101),[44] and in surface-modified TiO_2.[46,47]

First, we consider the energies as discussed in the Methods section and as presented in Table 1. The vertical excitation

Table 1. Calculated Energies Involved in the Photoexcited Model of Rutile−Anatase Interface Models in eV[a]

interface model	$E^{vertical}$	E^{S-T}	E^{relax}
R(110)−A(101)	1.64	0.94	0.70
R(001)−A(100)	1.60	0.46	1.13

[a]The terms $E^{vertical}$, E^{S-T}, and E^{relax} are explained in the Methods Section.

energies, $E^{vertical}$, correspond to a simple VB−CB energy difference and are essentially identical for both interface models, as well as being smaller than the corresponding energy difference for single-phase rutile and anatase, which we have computed under the same computational setup as 2.11 and 2.20 eV. Thus, the interface formation will give a reduction in the band gap compared to single-phase TiO_2, which is explained by the shift of both the VB and CB as a result of interface formation.[29]

The magnitude of the singlet−triplet energy difference, E^{S-T}, shows a dependence on which rutile and anatase surfaces form the junction. The R(001)−A(100) interface shows a smaller energy difference than the R(110)−A(101) interface and undergoes stronger relaxations in the photoexcited state, as evidenced by the magnitude of the relaxation energies. This is the energy gained when the structure is relaxed in the "excited" state and localizes the electron and hole, which in turn creates a strong geometric distortion to accompany the polaron so formed.

In Figures 3 and 4 we show the atomic structure and the spin density of the photoexcited triplet state after ionic relaxation and highlight the Ti and O sites on which the charges localize in the R(110)−A(101) and R(001)−A(100) interfaces after relaxation. In discussing the charge localization we describe the corresponding Ti or O site according to the phase in which it is originally present. The spin density for the R(110)−A(101) interface shows that upon relaxation the excited electron localizes onto an interfacial Ti atom originally from the anatase phase, which is reduced from Ti^{4+} to Ti^{3+}. The computed Bader charge of 1.67 electrons and a spin magnetization of 0.95 electrons are typical of reduced Ti^{3+} species. The local geometry around the reduced Ti^{3+} site shows elongated $Ti^{3+}-O^{2-}$ distances of 2.11, 2.09, 2.27, and 2.29 Å, compared to the original $Ti^{4+}-O^{2-}$ distances which ranged from 1.98 to 2.09 Å, and these are consistent with the elongated Ti−O bonds associated with a Ti^{3+} species. This Ti atom is one of the 4-coordinate Ti atoms present in the interfacial region, as discussed in Section 2.1.

The nature of the valence band hole in this interface is not as simple. The hole is spread over two interfacial oxygen atoms (indicated in Figure 3(b)), one of which was originally in the rutile phase and the other of which was originally in the anatase phase. The computed Bader charges are 7.0 electrons, and the spin magnetizations are 0.47 and 0.49 electrons, which are consistent with partial localization of the valence band hole over the two oxygen sites. Examining the geometry the O^- originating from rutile has $Ti-O^-$ distances of 2.04 and 1.99 Å,
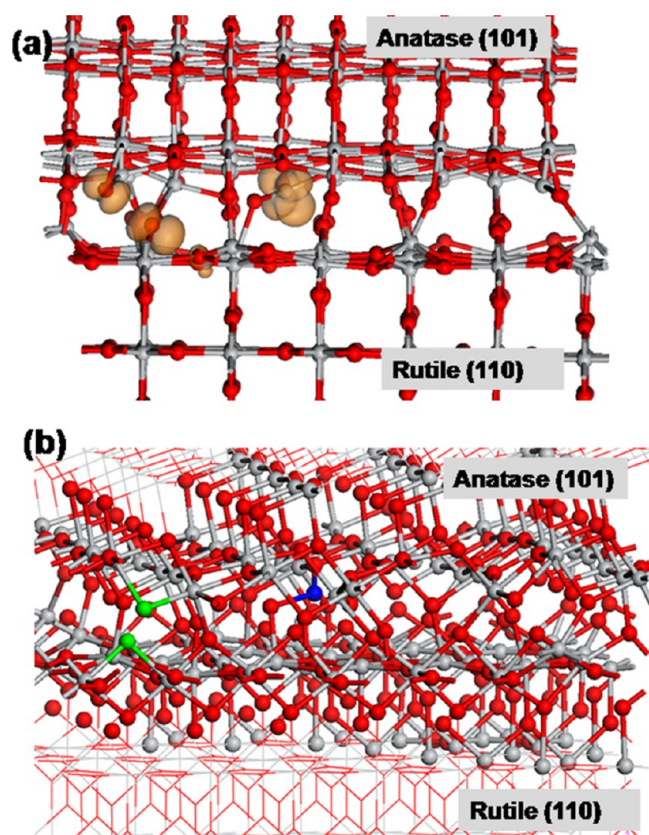
Figure 3. (a) Spin density plot of the interface in the triplet model for the R(110)−A(101) interfacial structure. (b) Local geometry around the photoexcited electron and hole, in which the blue sphere indicates the Ti sites carrying the electron and the green spheres indicate oxygen where the hole localizes. Spin density isosurfaces enclose volumes of up to 0.02 e/Å³.

Figure 4. (a) Spin density plot of the interface in triplet model for the R(001)−A(100) interfacial structure. (b) Local geometry around the photoexcited electron and hole, in which the blue sphere indicates the Ti sites carrying the electron and the green spheres indicate oxygen where the hole localizes. Spin density isosurfaces enclose volumes of up to 0.02 e/Å³.

while around the O⁻ site originating from anatase the Ti−O⁻ distances are 2.01 and 2.05 Å. The elongated Ti−O bonds are consistent with the presence of an oxygen hole. These findings finally resolve the outstanding uncertain interpretation of EPR data where the hole signals are not sufficiently resolved to confirm whether the hole is trapped on anatase, rutile, or some combination[16] by showing that the hole is spread over both anatase and rutile.

In the R(001)−A(100) interface model, the electron is localized on a Ti site originating from the rutile phase, while the VB hole is spread over two oxygen sites in the interface region; both oxygen sites originate in the rutile phase. Given that the VB and CB alignments suggest the opposite charge localization, this result shows that the significant relaxations within the interface upon formation of the excited state, as evidenced by the relaxation energy in Table 1, play a determining role in the final location of the electron and hole and not taking this into account can result in an incorrect interpretation. Thus, the analysis of bulk energy band alignments, without taking the interface into account, fails to capture this local behavior.

Finally, given the potential dependence of key properties of TiO₂ on the value of U, as described earlier, we have run again the R(001)−A(100) interface model with a different value of U on the Ti 3d states, that is, 3.9 eV, as suggested for anatase in ref 42, which captures electron delocalization in bulk anatase with an oxygen vacancy. Figure 5 shows the spin density for the relaxed triplet state with this DFT+U setup. Comparison with
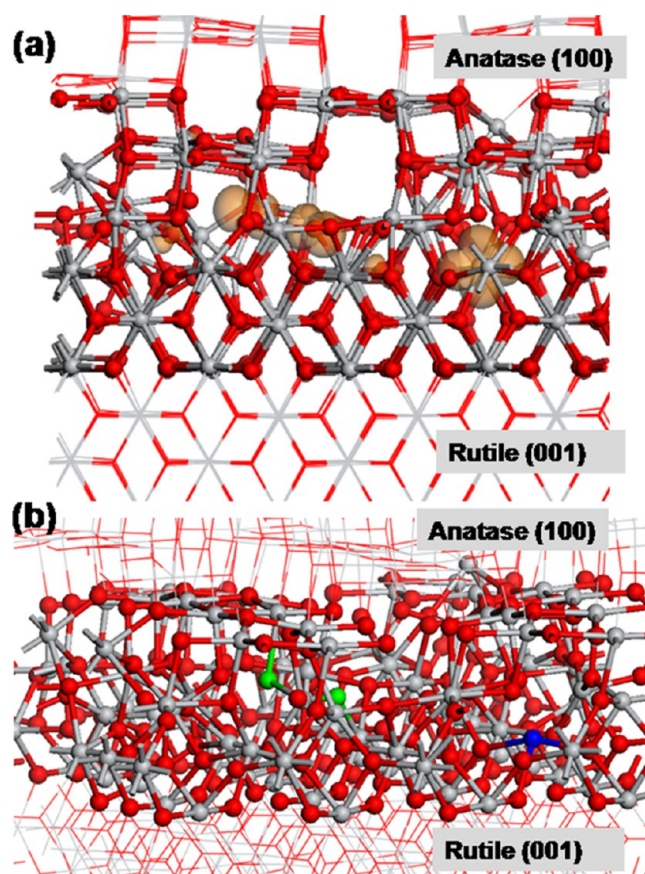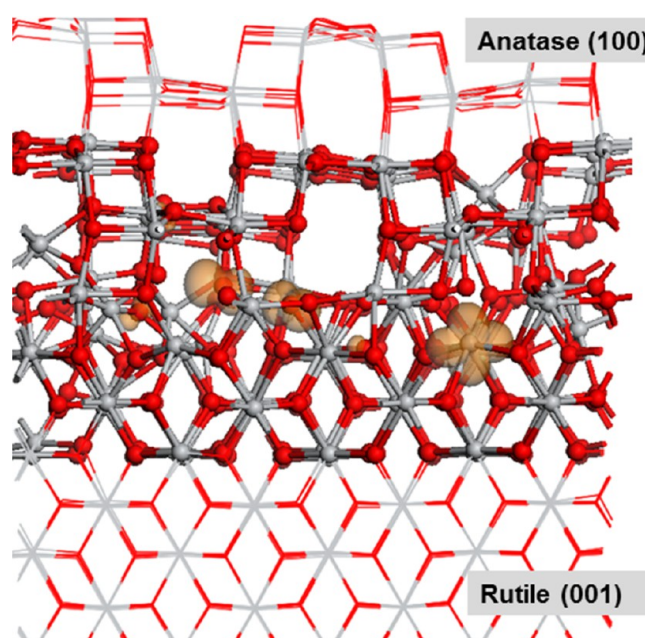

Figure 5. Spin density plot of the triplet model for the R(001)−A(100) interfacial structure, with U = 3.9 eV applied to the Ti 3d states. Spin density isosurfaces enclose volumes of up to 0.02 e/Å³.
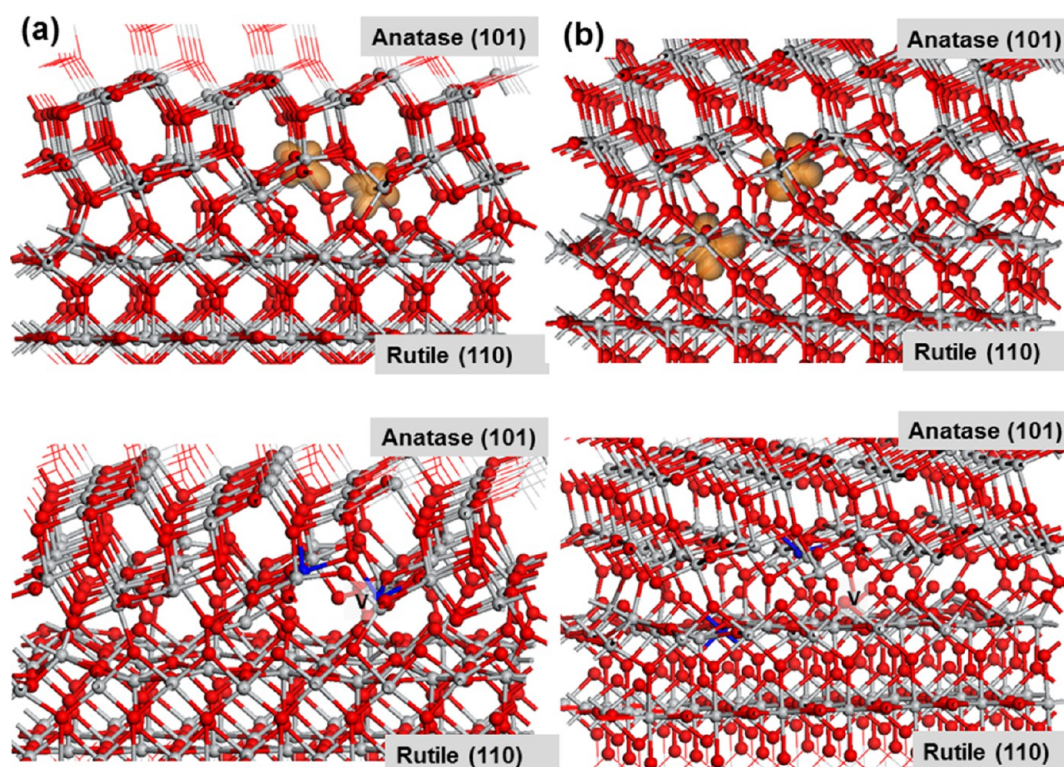
Figure 6. Top panels: Spin density for an O vacancy originating from (a) the anatase phase and (b) the rutile phase. Spin density isosurfaces enclose volumes of up to 0.02 e/Å³. Bottom panels: The local geometry, with the reduced Ti species indicated by blue spheres and the vacancy site by a "V".

Figure 4 shows that the choice of U has no impact on electron and hole localization—the electron is found on a Ti site in the interface, originating from the rutile phase, and the hole is localized over two interface oxygen atoms. Thus, the effect of the value of U (when using typical literature values) on electron and hole localization in these composite structures is negligible. This arises from the interface atomic structure being heavily distorted compared to the perfect bulk or extended surfaces, leading to formation of low coordinated Ti which are then able to trap electrons.

Upon examining the nature of the Ti and O species carrying the electron and the hole, the Ti site is reduced to Ti^{3+}, with $Ti^{3+}-O^{2-}$ distances of 1.99, 2.09, 2.02, and 2.09 Å, and this Ti was identified in Figure 2 as a 4-coordinated Ti site. Again, a simple analysis of bulk band offsets cannot capture the importance of the low coordinated interfacial sites, in particular low coordinated Ti, and it is these sites that are key in charge localization. The oxygen atoms that carry the hole have $Ti-O^-$ distances of 1.95 and 2.03 Å for one oxygen and 2.01 and 2.07 Å for the second oxygen. Similar to the R(110)−A(101) interface, Bader charges and spin magnetizations are typical of reduced Ti^{3+} species and hole carrying oxygen.

3.3. Interfacial Oxygen Vacancy Formation in Mixed-Phase TiO₂. To examine the formation of simple point defects in the interfaces, we consider the example of the R(110)−A(101) interface and the explicit formation of interfacial oxygen vacancies. We consider removal of interfacial oxygen originating from the rutile phase and from the anatase phase and relax the defective structure in each case.

Figure 6 shows the atomic structure and the spin density for an oxygen vacancy originating in the anatase (Figure 6(a)) and rutile (Figure 6(b)) phases; the vacancy site is indicated with a "V". The formation energy for an interfacial oxygen vacancy originating from anatase is +0.75 eV, while for an interfacial oxygen vacancy that originates from the rutile phase the vacancy formation energy is +2.08 eV. Oxygen vacancy defects are therefore more likely to form in the interfacial region of mixed-phase TiO_2 than in the bulk region of the pure phases. Additionally, loss of interfacial oxygen originating in the anatase phase is more likely.

After formation of the neutral oxygen vacancy, two Ti atoms are reduced from Ti^{4+} to Ti^{3+}, with the location of reduced Ti^{3+} species depending on the phase from which oxygen is removed. The anatase vacancy site results in formation of two Ti^{3+} species originating in the anatase phase: one Ti^{3+} species is present in the interface, and the second Ti^{3+} site is in the next sublayer away from the interface. In removing oxygen from the rutile phase, the reduced Ti^{3+} species are localized onto one interfacial Ti site originating from anatase and a second Ti site originating from rutile.

The local atomic geometry for both defective interfaces shows that the reduced Ti^{3+} species are 3- or 4-fold coordinated. For the more stable vacancy, the $Ti^{3+}-O$ distances are 2.11, 2.09, 2.03, and 2.03 Å (interfacial Ti) and 2.06, 2.05, 2.03, and 2.00 Å (sublayer Ti), while for the less stable vacancy, the $Ti^{3+}-O$ distances are 2.06, 1.96, and 1.93 Å (in anatase) and 2.11, 2.08, 2.04, and 1.98 Å (in rutile).

The relatively small vacancy formation energy indicates that oxygen vacancy defects could be present after the synthesis of mixed-phase films. Given that the vacancies are more likely to originate from the anatase phase, together with formation of Ti^{3+} in anatase, this makes these oxygen vacancies strong candidates for the trap states postulated to originate from anatase, as discussed in experimental work.[27]

4. CONCLUSIONS

We explore in detail the localization of photoexcited charges and the electrons released upon oxygen vacancy formation in rutile−anatase TiO_2 composites by modeling fully relaxed interfaces between the phases. This resolves the interpretation of previously unexplained experimental findings for the first time.

Thus, the key results that arise from these calculations of rutile−anatase interfaces are: (1) Electrons localize into low coordinated Ti sites in the interfaces, so that these special sites will be key in the activity of mixed-phase TiO_2. (2) Hole localization is not confined to a single phase, but the hole can be shared by two oxygens originating from different phases. (3) Formation of point defects such as oxygen vacancies is significantly more favorable in the heterojunction than in single-phase TiO_2. (4) Bulk band alignments do not always give a consistent indication of electron localization. The precise TiO_2 surfaces involved in the mixed phase can determine the electron and hole localization, which cannot be captured by simple bulk calculations. The properties of the interface therefore drive the performance of mixed-phase TiO_2, by determining band alignments and the localization of charge after excitation and point defect formation. The fate of photoexcited charges in TiO_2 composite materials is therefore controlled by the structural details of the disordered interface to a far greater extent than previously recognized; in particular, we note the key role of undercoordinated interfacial atomic sites. Consequently, the enhanced activity of TiO_2 composite materials is determined more by the local structure of the disordered interfacial region that can stabilize a higher charge density than by the direction of charge transfer as predicted by energy band offsets.

■ AUTHOR INFORMATION

Corresponding Author
*E-mail: michael.nolan@tyndall.ie.

Notes
The authors declare no competing financial interest.

■ REFERENCES

(1) Vinodgopal, K.; Bedja, I.; Kamat, P. V. Nanostructured Semiconductor Films for Photocatalysis. Photoelectrochemical Behavior of SnO_2/TiO_2 Composite Systems and Its Role in Photocatalytic Degradation of a Textile Azo Dye. *Chem. Mater.* **1996**, *8*, 2180−2187.

(2) Liang, Y. T.; Vijayan, B. K.; Lyandres, O.; Gray, K. A.; Hersam, M. C. Effect of Dimensionality on the Photocatalytic Behavior of Carbon−Titania Nanosheet Composites: Charge Transfer at Nanomaterial Interfaces. *J. Phys. Chem. Lett.* **2012**, *3*, 1760−1765.

(3) Jin, Z.; Li, Q.; Zheng, X.; Xi, C.; Wang, C.; Zhang, H.; Feng, L.; Wang, H.; Chen, Z.; Jiang, Z. Surface Properties of Pt-CdS and Mechanism of Photocatalytic Dehydrogenation of Aqueous Alcohol. *J. Photochem. Photobiol., A* **1993**, *71*, 85−96.

(4) Navalon, S.; de Miguel, M.; Martin, R.; Alvaro, M.; Garcia, H. Enhancement of the Catalytic Activity of Supported Gold Nanoparticles for the Fenton Reaction by Light. *J. Am. Chem. Soc.* **2011**, *133*, 2218−2226.

(5) Uchihara, T.; Matsumura, M.; Yamamoto, A.; Tsubomura, H. Effect of Platinum Loading on the Photocatalytic Activity and Luminescence of Cadmium Sulfide Powder. *J. Phys. Chem.* **1989**, *93*, 5870−5874.

(6) Wang, D.; Hisatomi, T.; Takata, T.; Pan, C.; Katayama, M.; Kubota, J.; Domen, K. Core/Shell Photocatalyst with Spatially Separated Co-Catalysts for Efficient Reduction and Oxidation of Water. *Angew. Chem., Int. Ed.* **2013**, *52*, 11252−11256.

(7) Wang, W.; Zhang, J.; Chen, F.; He, D.; Anpo, M. Preparation and Photocatalytic Properties of Fe3+-Doped $Ag@TiO_2$ Core−Shell Nanoparticles. *J. Colloid Interface Sci.* **2008**, *323*, 182−186.

(8) Ismail, A. A.; Bahnemann, D. W.; Al-Sayari, S. A. Synthesis and Photocatalytic Properties of Nanocrystalline Au, Pd and Pt Photodeposited onto Mesoporous RuO_2-TiO_2 Nanocomposites. *Appl. Catal., A* **2012**, *431−432*, 62−68.

(9) Yao, Y.; Li, G.; Ciston, S.; Lueptow, R. M.; Gray, K. A. Photoreactive TiO_2/Carbon Nanotube Composites: Synthesis and Reactivity. *Environ. Sci. Technol.* **2008**, *42*, 4952−4957.

(10) Li, G.; Dimitrijevic, N. M.; Chen, L.; Rajh, T.; Gray, K. A. Role of Surface/Interfacial Cu^{2+} Sites in the Photocatalytic Activity of Coupled CuO-TiO_2 Nanocomposites. *J. Phys. Chem. C* **2008**, *112*, 19040−19044.

(11) Wang, C.; Thompson, R. L.; Baltrus, J.; Matranga, C. Visible Light Photoreduction of CO_2 Using CdSe/Pt/TiO_2 Heterostructured Catalysts. *J. Phys. Chem. Lett.* **2009**, *1*, 48−53.

(12) Abou Asi, M.; He, C.; Su, M.; Xia, D.; Lin, L.; Deng, H.; Xiong, Y.; Qiu, R.; Li, X.-Z. Photocatalytic Reduction of CO_2 to Hydrocarbons using AgBr/TiO_2 Nanocomposites under Visible Light. *Catal. Today* **2011**, *175*, 256−263.

(13) Kamat, P. V. Graphene-Based Nanoarchitectures. Anchoring Semiconductor and Metal Nanoparticles on a Two-Dimensional Carbon Support. *J. Phys. Chem. Lett.* **2009**, *1*, 520−527.

(14) Kho, Y. K.; Iwase, A.; Teoh, W. Y.; Mädler, L.; Kudo, A.; Amal, R. Photocatalytic H_2 Evolution over TiO_2 Nanoparticles. The Synergistic Effect of Anatase and Rutile. *J. Phys. Chem. C* **2010**, *114*, 2821−2829.

(15) Zhang, J.; Xu, Q.; Feng, Z.; Li, M.; Li, C. Importance of the Relationship between Surface Phases and Photocatalytic Activity of TiO_2. *Angew. Chem., Int. Ed.* **2008**, *47*, 1766−1769.

(16) Hurum, D. C.; Agrios, A. G.; Gray, K. A.; Rajh, T.; Thurnauer, M. C. Explaining the Enhanced Photocatalytic Activity of Degussa P25 Mixed-Phase TiO_2 Using EPR. *J. Phys. Chem. B* **2003**, *107*, 4545−4549.

(17) Xiong, G.; Shao, R.; Droubay, T. C.; Joly, A. G.; Beck, K. M.; Chambers, S. A.; Hess, W. P. Photoemission Electron Microscopy of TiO_2 Anatase Films Embedded with Rutile Nanocrystals. *Adv. Funct. Mater.* **2007**, *17*, 2133−2138.

(18) Kavan, L.; Grätzel, M.; Gilbert, S. E.; Klemenz, C.; Scheel, H. J. Electrochemical and Photoelectrochemical Investigation of Single-Crystal Anatase. *J. Am. Chem. Soc.* **1996**, *118*, 6716−6723.

(19) Komaguchi, K.; Nakano, H.; Araki, A.; Harima, Y. Photoinduced Electron Transfer from Anatase to Rutile in Partially Reduced TiO_2 (P-25) nanoparticles: An ESR study. *Chem. Phys. Lett.* **2006**, *428*, 338−342.

(20) Zhang, X.; Lin, Y.; He, D.; Zhang, J.; Fan, Z.; Xie, T. Interface Junction at Anatase/Rutile in Mixed-Phase TiO_2: Formation and

Photo-Generated Charge Carriers Properties. *Chem. Phys. Lett.* **2011**, *504*, 71−75.

(21) Kawahara, T.; Konishi, Y.; Tada, H.; Tohge, N.; Nishii, J.; Ito, S. A Patterned TiO_2(Anatase)/TiO_2(Rutile) Bilayer-Type Photocatalyst: Effect of the Anatase/Rutile Junction on the Photocatalytic Activity. *Angew. Chem., Int. Ed.* **2002**, *41*, 2811−2813.

(22) Miyagi, T.; Kamei, M.; Mitsuhashi, T.; Ishigaki, T.; Yamazaki, A. Charge Separation at the Rutile/Anatase Interface: a Dominant Factor of Photocatalytic Activity. *Chem. Phys. Lett.* **2004**, *390*, 399−402.

(23) Ohno, T.; Sarukawa, K.; Matsumura, M. Photocatalytic Activities of Pure Rutile Particles Isolated from TiO_2 Powder by Dissolving the Anatase Component in HF Solution. *J. Phys. Chem. B* **2001**, *105*, 2417−2420.

(24) Emeline, A. V.; Smirnova, L. G.; Kuzmin, G. N.; Basov, L. L.; Serpone, N. Spectral Dependence of Quantum Yields in Gas−Solid Heterogeneous Photosystems: Influence of Anatase/Rutile Content on the Photostimulated Adsorption of Dioxygen and Dihydrogen on Titania. *J. Photochem. Photobiol., A* **2002**, *148*, 97−102.

(25) Hurum, D. C.; Agrios, A. G.; Crist, S. E.; Gray, K. A.; Rajh, T.; Thurnauer, M. C. Probing Reaction Mechanisms in Mixed Phase TiO_2 by EPR. *J. Electron Spectrosc. Relat. Phenom.* **2006**, *150*, 155−163.

(26) Hurum, D. C.; Gray, K. A.; Rajh, T.; Thurnauer, M. C. Recombination Pathways in the Degussa P25 Formulation of TiO_2: Surface versus Lattice Mechanisms. *J. Phys. Chem. B* **2005**, *109*, 977−980.

(27) Leytner, S.; Hupp, J. T. Evaluation of the Energetics of Electron Trap States at the Nanocrystalline Titanium Dioxide/Aqueous Solution Interface via Time-Resolved Photoacoustic Spectroscopy. *Chem. Phys. Lett.* **2000**, *330*, 231−236.

(28) Deák, P.; Aradi, B. l.; Frauenheim, T. Band Lineup and Charge Carrier Separation in Mixed Rutile-Anatase Systems. *J. Phys. Chem. C* **2011**, *115*, 3443−3446.

(29) Garcia, J. C.; Nolan, M.; Deskins, N. A. The Nature of Interfaces and Charge Trapping Sites in Photocatalytic Mixed-Phase TiO_2 from First Principles Modeling. *J. Chem. Phys.* **2015**, *142*, 024708/1−024708/10.

(30) Kullgren, J.; Huy, H. A.; Aradi, B.; Frauenheim, T.; Deák, P. Theoretical Study of Charge Separation at the Rutile−Anatase Interface. *Phys. Status Solidi RRL* **2014**, *8*, 566−570.

(31) Pfeifer, V.; Erhart, P.; Li, S.; Rachut, K.; Morasch, J.; Brötz, J.; Reckers, P.; Mayer, T.; Rühle, S.; Zaban, A.; Sero Mora, I.; Bisquert, J.; Jaegermann, W.; Klein, A. Energy Band Alignment between Anatase and Rutile TiO_2. *J. Phys. Chem. Lett.* **2013**, *4*, 4182−4187.

(32) Scanlon, D. O.; Dunnill, C. W.; Buckeridge, J.; Shevlin, S. A.; Logsdail, A. J.; Woodley, S. M.; Catlow, C. R. A.; Powell, M. J.; Palgrave, R. G.; Parkin, I. P.; Watson, G. W.; Keal, T. W.; Sherwood, P.; Walsh, A.; Sokol, A. A. Band Alignment of Rutile and Anatase TiO_2. *Nat. Mater.* **2013**, *12*, 798−801.

(33) Peacock, P. W.; Robertson, J. Bonding, Energies, and Band Offsets of Si-ZrO_2 and HfO_2 Gate Oxide Interfaces. *Phys. Rev. Lett.* **2004**, *92*, 057601.

(34) Tao, J.; Batzill, M. Role of Surface Structure on the Charge Trapping in TiO_2 Photocatalysts. *J. Phys. Chem. Lett.* **2010**, *1*, 3200−3206.

(35) Zhang, J.; Li, M.; Feng, Z.; Chen, J.; Li, C. UV Raman Spectroscopic Study on TiO_2. I. Phase Transformation at the Surface and in the Bulk. *J. Phys. Chem. B* **2005**, *110*, 927−935.

(36) Zhuang, J.; Dai, W.; Tian, Q.; Li, Z.; Xie, L.; Wang, J.; Liu, P.; Shi, X.; Wang, D. Photocatalytic Degradation of RhB over TiO_2 Bilayer Films: Effect of Defects and Their Location. *Langmuir* **2010**, *26*, 9686−9694.

(37) Pan, X.; Yang, M.-Q.; Fu, X.; Zhang, N.; Xu, Y.-J. Defective TiO_2 with Oxygen Vacancies: Synthesis, Properties and Photocatalytic Applications. *Nanoscale* **2013**, *5*, 3601−3614.

(38) Zhuang, J.; Weng, S.; Dai, W.; Liu, P.; Liu, Q. Effects of Interface Defects on Charge Transfer and Photoinduced Properties of TiO_2 Bilayer Films. *J. Phys. Chem. C* **2012**, *116*, 25354−25361.

(39) Kresse, G.; Furthmüller, J. Efficiency of Ab-Initio Total Energy Calculations for Metals and Semiconductors using a Plane-Wave Basis Set. *Comput. Mater. Sci.* **1996**, *6*, 15−50.

(40) Kresse, G.; Hafner, J. Ab Initio Molecular Dynamics for Liquid Metals. *Phys. Rev. B: Condens. Matter Mater. Phys.* **1993**, *47*, 558−561.

(41) Kresse, G.; Joubert, D. From Ultrasoft Pseudopotentials to the Projector Augmented-Wave Method. *Phys. Rev. B: Condens. Matter Mater. Phys.* **1999**, *59*, 1758−1775.

(42) Perdew, J. P.; Burke, K.; Ernzerhof, M. Generalized Gradient Approximation Made Simple. *Phys. Rev. Lett.* **1996**, *77*, 3865−3868.

(43) Setvin, M.; Franchini, C.; Hao, X.; Schmid, M.; Janotti, A.; Kaltak, M.; Van de Walle, C. G.; Kresse, G.; Diebold, U. Direct View at Excess Electrons in TiO_2 Anatase and Rutile. *Phys. Rev. Lett.* **2014**, *113*, 086402/1−086402/4.

(44) Deskins, N. A.; Kerisit, S.; Rosso, K. M.; Dupuis, M. Molecular Dynamics Characterization of Rutile-Anatase Interfaces. *J. Phys. Chem. C* **2007**, *111*, 9290−9298.

(45) Di Valentin, C.; Selloni, A. Bulk and Surface Polarons in Photoexcited Anatase TiO_2. *J. Phys. Chem. Lett.* **2011**, *2*, 2223−2228.

(46) Jedidi, A.; Markovits, A.; Minot, C.; Bouzriba, S.; Abderraba, M. Modeling Localized Photoinduced Electrons in Rutile-TiO_2 Using Periodic DFT+U Methodology. *Langmuir* **2010**, *26*, 16232−16238.

(47) Iwaszuk, A.; Nolan, M. SnO-Nanocluster Modified Anatase TiO_2 Photocatalyst: Exploiting the Sn(II) Lone Pair for a new Photocatalyst Material with Visible Light Absorption and Charge Carrier Separation. *J. Mater. Chem. A* **2013**, *1*, 6670−6677.

(48) Nolan, M. First-Principles Prediction of New Photocatalyst Materials with Visible-Light Absorption and Improved Charge Separation: Surface Modification of Rutile TiO_2 with Nanoclusters of MgO and Ga_2O_3. *ACS Appl. Mater. Interfaces* **2012**, *4*, 5863−5871.

(49) Pan, J.; Liu, G.; Lu, G. Q.; Cheng, H.-M. On the True Photoreactivity Order of {001}, {010}, and {101} Facets of Anatase TiO_2 Crystals. *Angew. Chem., Int. Ed.* **2011**, *50*, 2133−2137.

(50) Iwaszuk, A.; Mulheran, P. A.; Nolan, M. TiO_2 Nanocluster Modified-Rutile TiO_2 Photocatalyst: a First Principles Investigation. *J. Mater. Chem. A* **2013**, *1*, 2515−2525.

(51) Nolan, M.; Iwaszuk, A.; Gray, K. A. Localization of Photoexcited Electrons and Holes on Low Coordinated Ti and O Sites in Free and Supported TiO_2 Nanoclusters. *J. Phys. Chem. C* **2014**, *118*, 27890−27900.